






RESEARCH ARTICLE | JANUARY 04 2024

NMR spectroscopy of a ^{18}O -labeled rhodium paddlewheel complex: Isotope shifts, ^{103}Rh – ^{103}Rh spin–spin coupling, and ^{103}Rh singlet NMR

Harry Harbor-Collins ; Mohamed Sabba; Christian Bengs ; Gamal Moustafa; Markus Leutzsch ; Malcolm H. Levitt  



J. Chem. Phys. 160, 014305 (2024)

<https://doi.org/10.1063/5.0182233>



View
Online



Export
Citation

CrossMark



The Journal of Chemical Physics
2024 Emerging Investigators
Special Collection

Submit Today

 AIP
Publishing

 AIP
Publishing

NMR spectroscopy of a ^{18}O -labeled rhodium paddlewheel complex: Isotope shifts, ^{103}Rh – ^{103}Rh spin–spin coupling, and ^{103}Rh singlet NMR

Cite as: J. Chem. Phys. 160, 014305 (2024); doi: 10.1063/5.0182233

Submitted: 18 October 2023 • Accepted: 10 December 2023 •

Published Online: 4 January 2024



View Online



Export Citation



CrossMark

Harry Harbor-Collins,¹  Mohamed Sabba,¹ Christian Bengs,¹  Gamal Moustafa,¹ Markus Leutzsch,² 
and Malcolm H. Levitt^{1,a)} 

AFFILIATIONS

¹School of Chemistry, University of Southampton, Southampton SO17 1BJ, United Kingdom

²Max-Planck-Institut für Kohlenforschung, Kaiser-Wilhelm-Platz 1, Mülheim an der Ruhr 45470, Germany

^{a)}Author to whom correspondence should be addressed: mhl@soton.ac.uk

ABSTRACT

Despite the importance of rhodium complexes in catalysis, and the favorable 100% natural abundance of the spin-1/2 ^{103}Rh nucleus, there are few reports of ^{103}Rh nuclear magnetic resonance (NMR) parameters in the literature. In part, this is the consequence of the very low gyromagnetic ratio of ^{103}Rh and its dismal NMR sensitivity. In a previous paper [Harbor-Collins *et al.*, J. Chem. Phys. **159**, 104 307 (2023)], we demonstrated an NMR methodology for ^1H -enhanced ^{103}Rh NMR and demonstrated an application to the ^{103}Rh NMR of the dirhodium formate paddlewheel complex. In this paper, we employ selective ^{18}O labeling to break the magnetic equivalence of the ^{103}Rh spin pair of dirhodium formate. This allows the estimation of the ^{103}Rh – ^{103}Rh spin–spin coupling and provides access to the ^{103}Rh singlet state. We present the first measurement of a ^{18}O -induced ^{103}Rh secondary isotope shift as well as the first instance of singlet order generated in a ^{103}Rh spin pair. The field-dependence of ^{103}Rh singlet relaxation is measured by field-cycling NMR experiments.

© 2024 Author(s). All article content, except where otherwise noted, is licensed under a Creative Commons Attribution (CC BY) license (<http://creativecommons.org/licenses/by/4.0/>). <https://doi.org/10.1063/5.0182233>

I. INTRODUCTION

Rhodium paddlewheel complexes are of profound importance in the field of catalysis^{1–9} and were some of the earliest anticancer agents to be studied.^{10–12} The range of roles played by these complexes is the result of their fascinating properties that, over the years, have attracted fervent interest and investigation by a variety of methods.^{13–20}

An excellent probe of the properties of these complexes is ^{103}Rh nuclear magnetic resonance (NMR). Despite the rich information provided by this technique, it is sparsely attempted due to a host of onerous experimental challenges, arising from the extremely low gyromagnetic ratio of ^{103}Rh . Nevertheless, it has been recently demonstrated that high-quality ^{103}Rh NMR spectra can be readily obtained on commercial NMR probes with a combination of (i) two-dimensional heteronuclear multiple-quantum techniques²¹ and (ii) polarization transfer methods.²²

An early controversy^{9,23} on the nature of the rhodium–rhodium bond in paddlewheel complexes was resolved via the use of ^{103}Rh NMR spectroscopy to measure a homonuclear ^{103}Rh – ^{103}Rh J-coupling,²⁴ in a highly asymmetric complex. However, in *symmetric* complexes, where all bridging ligands are identical, the chemical equivalence of the ^{103}Rh spins, at first sight, appears to imply that an observation of a ^{103}Rh – ^{103}Rh J-coupling by NMR would be symmetry-forbidden.

Here, we introduce a further innovation—the use of selective ^{18}O labeling to break the symmetry of symmetric paddlewheel complexes through secondary isotope shifts, by analogy with previous work on ^{18}O -enriched ^{13}C compounds.^{25,26} We measure a ^{18}O -induced secondary isotope shift of ^{103}Rh , $\Delta^{103}\text{Rh}(^{16}\text{O}, ^{18}\text{O})$, for the first time. We show that the symmetry-breaking by the secondary isotope shifts allows (i) the estimation of ^{103}Rh – ^{103}Rh J-couplings in symmetric paddlewheel complexes and (ii) the study of long-lived ^{103}Rh – ^{103}Rh singlet order.

II. EXPERIMENTAL

A. Sample

^{18}O -labeled rhodium formate ($\text{Rh}_2(\text{HCO}_2)_4$) was prepared by the procedure described in the supplementary material.

Although the Rh(II) formate dimer contains four formate ligands, only one of these was ^{18}O -enriched. The chosen synthetic route statistically enriched the two oxygen atoms of this single formate residue to $\sim 45\%$ with ^{18}O , with the oxygen atoms of the three other formate residues kept as the usual ^{16}O isotope. As a result, the compound that was used contains a statistical mixture of three different major isotopologues, denoted here by **I**, **II**, **III** as shown in Fig. 1. As shown below, the statistical abundances in solution are approximately 30%, 50%, 20% for the isotopologues **I**, **II**, **III**, respectively.

Experiments were performed on a saturated (~ 10 mM) solution of the isotopic mixture shown in Fig. 1, dissolved in 500 μl deuterated tetrahydrofuran ($\text{THF-}d_8$) contained in a Wilmad LPV 5 ml sample tube. In solution, $\text{THF-}d_8$ molecules coordinate to the axial positions of the paddlewheel complex, as shown for species **II** in Table I.

Species **II** is of most importance for the study described here. The asymmetric $^1\Delta^{103}\text{Rh}(^{16}\text{O}, ^{18}\text{O})$ isotope shift renders the ^{103}Rh nuclei chemically inequivalent. The inequivalence provides access to the ^{103}Rh - ^{103}Rh J-couplings, and to ^{103}Rh - ^{103}Rh singlet order. The parameters of the spin system of **II**, as estimated through the experiments described below, are given in Table I.

B. ^{18}O secondary isotope convention

All secondary isotope shifts induced by replacing ^{16}O by ^{18}O are reported here using the commonly used convention,²⁷ as follows:

$${}^n\Delta X(^{16}\text{O}, ^{18}\text{O}) = \delta_X(^{16}\text{O}) - \delta_X(^{18}\text{O}), \quad (1)$$

where X is the observed nuclide and n is the number of bonds between ^{18}O and the observed nucleus. This convention has a counterintuitive sign definition but is popular, presumably because it usually leads to positive values for $^1\Delta$.

Some papers use a convention that has the opposite sign.²⁵

C. Solution NMR

^1H and ^{103}Rh spectra were acquired at a magnetic field strength of 9.4 T using a standard commercial Bruker 5 mm NMR BBO probe ($^1\text{H}/^2\text{H}/^{109}\text{Ag}$ - ^{31}P) equipped with a z-gradient with a maximum strength of 50 G cm^{-1} .

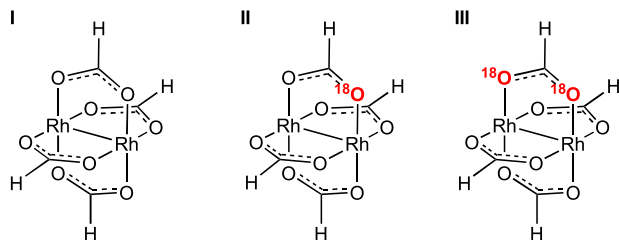


FIG. 1. Molecular structures of the three rhodium formate isotopologues present in the sample. Oxygen atoms with no annotation are the usual ^{16}O isotope.

TABLE I. Molecular structure of a ^{18}O -labeled rhodium formate paddlewheel complex (species **II** in Fig. 1) with its relevant NMR parameters in a magnetic field of 9.4 T, as determined by the experiments described in this paper. The ^{103}Rh - ^{103}Rh spin pair is shown in blue. Solvent $\text{THF-}d_8$ molecules occupy axial sites. The chemical shift difference $\omega_\Delta/(2\pi)$ between the two ^{103}Rh nuclei is equal to the sum of the one-bond and two-bond ^{18}O -induced secondary isotope shifts. The singlet-triplet mixing angle θ_{ST} is defined in Eq. (10).

${}^3J_{\text{RhRh}}/\text{Hz}$	4.7 ± 0.1
${}^1J_{\text{RhRh}}/\text{Hz}$	26.0 ± 0.1
$\Delta^{103}\text{Rh}(^{16}\text{O}, ^{18}\text{O})/\text{ppb}$	1450 ± 1
$\omega_\Delta/(2\pi)/\text{Hz}$ [$\text{@}9.4$ T]	18.5 ± 0.1
$\theta_{\text{ST}}/^\circ$	35.4 ± 0.2

^1H resonances are referenced to the absolute frequency 400.143 00 MHz; ^{103}Rh resonances are referenced to the absolute frequency 12.644 52 MHz, which is proportional to the ^1H frequency through the ratio $\Xi(^{103}\text{Rh}) = 3.16\%$, as per a common convention.¹³

For details of the probe tuning and radiofrequency filters, see Ref. 22. The radiofrequency amplitudes were adjusted to give matched nutation frequencies of $\omega_{\text{nut}}/(2\pi) \simeq 4$ kHz for the ^1H and ^{103}Rh channels, corresponding to a 90° pulse durations of 62.5 μs in both cases.

^{13}C spectra were acquired using a 5 mm Bruker probe at 14.1 T and 298 K. ^{13}C resonances are referenced to the absolute frequency 150.903 00 MHz.

Field-cycling experiments used rapid sample shuttling from inside the 9.4 T magnet bore to regions of lower field outside the magnet bore, using a motorized fast shuttling system based on the design by Kiryutin.²⁸ The shuttling time was kept constant at 1 s, in both directions. Shuttling from high to low field is initiated at 30 μs after the end of the previous pulse sequence. The high-field pulse sequence is resumed 15 μs after completion of the shuttling from low to high field. Further details on the shuttling trajectory and the time-dependence of the magnetic field during the shuttling are given in the supplementary material.

D. Pulse sequences

The pulse sequences have a modular design. Some modules were described in our previous paper.²² Some further modules are introduced here.

1. Standard modules

Details of the following modules are given in Ref. 22:

1. *Composite pulses* of the type BB1^{29,30} in which a simple pulse β_ϕ (where β is the flip angle and ϕ is the phase) is replaced by

$$(\beta/2)_\phi 180_{\phi+\theta_W} 360_{\phi+3\theta_W} 180_{\phi+\theta_W} (\beta/2)_\phi, \quad (2)$$

where $\theta_W = \arccos(-\beta/(4\pi))$. For $\pi/2$ and π flip angles, this corresponds to the following sequences:

$$90_\phi \rightarrow 45_\phi 180_{\phi+97.18} 360_{\phi+291.54} 180_{\phi+97.18} 45_\phi, \quad (3)$$

$$180_\phi \rightarrow 90_\phi 180_{\phi+104.48} 360_{\phi+313.43} 180_{\phi+104.48} 90_\phi. \quad (4)$$

Composite pulses are denoted by black rectangles in the pulse sequence diagrams.

2. *DualPol* pulse sequences for polarization transfer between ^1H and ^{103}Rh nuclei, consisting of synchronized PulsePol sequences^{31,32} applied simultaneously to the two channels (see Fig. 2 of Ref. 22). The use of DualPol is particularly important in the current context, since traditional INEPT-based methods^{33,34} have poor efficiency for the strongly coupled system of isotopologue II. All DualPol sequences used in the current work have a duration of 100 ms and are identical to those described in Ref. 22.
3. A ^1H *z-filter module*, which consists of a composite 180° ^1H pulse bracketed by two field-gradient pulses of opposite sign (see Fig. 4 of Ref. 22). This pulse sequence element suppresses signals that do not derive from ^1H z-magnetization in existence when the pulse sequence module is applied.
4. ^1H and ^{103}Rh *decoupling*, for experiments involving either ^1H or ^{103}Rh decoupling continuous wave decoupling was employed. For decoupling on the ^1H channel, the decoupling field corresponded to a nutation frequency of $\omega_{nut}/(2\pi) \approx 800$ Hz centered at 6.9 ppm. For decoupling on the ^{103}Rh channel, the decoupling field corresponded to a nutation frequency of $\omega_{nut}/(2\pi) \approx 160$ Hz centered at 7517.5 ppm.

2. Single-channel PulsePol

As discussed in Ref. 35, the PulsePol sequence, originally developed for polarization transfer between electron and nuclear spins in the solid state,^{31,32} may also be used for singlet-triplet conversion in solution NMR. Here, we use single-channel ^{103}Rh PulsePol sequences to convert ^{103}Rh longitudinal magnetization into ^{103}Rh - ^{103}Rh singlet order and back again.

The operation of PulsePol in the context of singlet-triplet conversion may be understood using symmetry-based recoupling theory, adapted from magic-angle-spinning solid-state NMR.³⁶ Within this interpretation, as described in Ref. 35, a pulse sequence is denoted RN_n^v , where N , n , and v are called symmetry numbers, with N constrained to be even. The sequence is based on a pulse sequence module called an *R*-element, which induces a rotation of the spins by an odd multiple of π about the rotating-frame x-axis. An example is given in Fig. 2, where the first three pulses and two delays constitute the *R*-element. A RN_n^v sequence consists of N *R*-elements, alternating between phases $\pm\pi v/N$ and timed to span n periods $\tau_j = |J|^{-1}$ of the homonuclear J-coupling J . The sequence used in this paper is shown in Fig. 2. The sequence has $R4_1^1$ symmetry but uses a variant of the construction procedure, called riffling, which endows the sequence with more robustness, as described in Ref. 35. In this

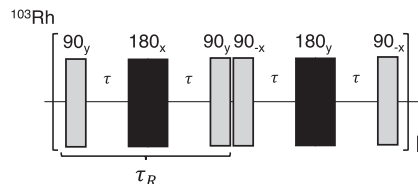


FIG. 2. PulsePol sequence used for the interconversion of ^{103}Rh z-magnetization and ^{103}Rh - ^{103}Rh singlet order. In this work, the parameters were $\tau_R = 9.8$ ms and $n = 10$, giving a total of 10 *R*-elements with a total duration of 98 ms. The number of repetitions (“loops”) is denoted L . Black rectangles indicate composite π pulses [Eq. (4)]. Gray rectangles indicate simple $\pi/2$ pulses.

case, the alternating phase shifts are given by $\pm\pi v/N = \pm 45^\circ$. The phases in Fig. 2 are obtained by an additional global phase shift of $\pi/4$. The *R*-element duration, given by $\tau_R \approx n/(N|J_{\text{RhRh}}|)$ in the near-equivalence limit, was experimentally optimized to 9.8 ms. Here, J_{RhRh} is the one-bond J-coupling between the two ^{103}Rh nuclei. As shown in the Appendix, the optimal number of repetitions L for the generation of rhodium singlet order is given by

$$L \approx \text{round}\left(\frac{\pi}{4\sqrt{2}} \cot(\theta_{\text{ST}}) \csc^2\left(\frac{\pi n}{2N}\right)\right). \quad (5)$$

In the current case, the optimal number of repetitions is equal to 5 for a total of 10 *R*-elements with a combined duration of 98 ms.

3. Dual T_{00} filter

The standard single-channel T_{00} filter is a sequence of radiofrequency and field-gradient pulses, which, to a good approximation, selects spin operators transforming as a rank-0 spherical tensor operator, meaning that they are invariant to all three-dimensional rotations.^{25,37} For spin-1/2 pair systems, these are the unity operator and the scalar coupling operator, which corresponds to singlet order. The dual T_{00} filter, shown in Fig. 3, uses simultaneous T_{00} filter sequences on two radiofrequency channels. This module selects for spin order terms that are invariant under all rotations of either

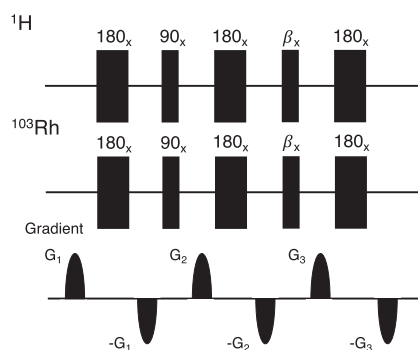


FIG. 3. Dual T_{00} filter for the selection of rank-0 spin order, using bipolar gradient pulses and radiofrequency pulses. β_x denotes a pulse with phase 0 with a flip angle of 54.74° (i.e., the magic angle). The gradient strengths are given by $G_1 = 100\%$, $G_2 = 61.8\%$ and $G_3 = 38.2\%$ with respect to the maximum gradient strength of 50 G cm^{-1} . Each gradient pulse has a duration of 2 ms. The black rectangles indicate BB1 composite pulses [Eqs. (2)–(4)].

the ^{103}Rh or ^1H spin states. The selected spin operators are the unity operator, the operator for ^{103}Rh singlet order, ^1H singlet order, and in principle higher scalar combinations of the states of the four ^1H nuclei. In the current context, this filter sequence (i) selects for ^{103}Rh singlet order and (ii) suppresses residual ^1H longitudinal and transverse magnetization. The latter feature is especially important for removing undesired ^1H signals during the indirect detection of ^{103}Rh -derived signals through the ^1H channel.

The parameters of the dual T_{00} filter sequence used in this work are as follows: The gradient strengths are given by $G_1 = 100\%$, $G_2 = 61.8\%$, and $G_3 = 38.2\%$ with respect to the maximum gradient strength of 50 G cm^{-1} . The duration of the gradients was 2 ms. The flip angle β is given by the magic angle 54.74° .

4. S_2S' and $S'S$ sequences, and quasi-singlet eigenorder

The singlet and triplet states of spin-1/2 pairs are defined as follows:

$$\begin{aligned} |S_0\rangle &= \frac{1}{\sqrt{2}}(|\alpha\beta\rangle - |\beta\alpha\rangle) \\ |T_{+1}\rangle &= |\alpha\alpha\rangle \\ |T_0\rangle &= \frac{1}{\sqrt{2}}(|\alpha\beta\rangle + |\beta\alpha\rangle) \\ |T_{-1}\rangle &= |\beta\beta\rangle. \end{aligned} \quad (6)$$

Singlet order is the mean population difference between the singlet and triplet states and is represented by the operator Q_S , defined as follows:³⁸

$$Q_S = |S_0\rangle\langle S_0| - \frac{1}{3} \sum_{m=-1}^{+1} |T_m\rangle\langle T_m| = -\frac{4}{3} \mathbf{I}_1 \cdot \mathbf{I}_2. \quad (7)$$

In suitable systems displaying exact or near magnetic equivalence, the singlet order operator Q_S is a long-lived state of the system and may display an exceptionally long relaxation time.³⁸

As shown by the parameters in Table I, the relatively large $^1\Delta^{103}\text{Rh}$ (^{18}O) isotope shift takes the ^{103}Rh pair spin system of isotopologue **II** out of magnetic equivalence in high magnetic field. As a result, the singlet order operator Q_S is not preserved under free evolution at high field and displays a complex dynamical behavior. Moreover, although the ^{103}Rh spin pair shift difference may be suppressed via the application of a strong resonant spin locking field,³⁹ the low gyromagnetic ratio of ^{103}Rh would require the application of prohibitively high powers to achieve a field of appropriate strength, which was beyond the acceptable limits of our probe. Therefore, to keep the spin dynamics under control, we instead opted to prepare an alternative spin operator, denoted Q'_S , defined as follows:

$$Q'_S = |S_0\rangle\langle S_0|' - \frac{1}{3} \sum_{m=-1}^{+1} |T_m\rangle\langle T_m|', \quad (8)$$

where $\{|S_0\rangle', |T_{+1}\rangle', |T_0\rangle', |T_{-1}\rangle'\}$ are eigenstates of the spin Hamiltonian in high magnetic field. These Hamiltonian eigenstates are defined as follows:

$$\begin{aligned} |S_0\rangle' &= \cos\left(\frac{1}{2}\theta_{\text{ST}}\right)|S_0\rangle + \sin\left(\frac{1}{2}\theta_{\text{ST}}\right)|T_0\rangle, \\ |T_0\rangle' &= \cos\left(\frac{1}{2}\theta_{\text{ST}}\right)|T_0\rangle - \sin\left(\frac{1}{2}\theta_{\text{ST}}\right)|S_0\rangle, \\ |T_{\pm 1}\rangle' &= |T_{\pm 1}\rangle, \end{aligned} \quad (9)$$

where the singlet–triplet mixing angle θ_{ST} is defined as

$$\theta_{\text{ST}} = \tan^{-1}(\Delta/J). \quad (10)$$

Here, Δ is the isotropic shift difference and J is the internuclear J-coupling, both defined in units of Hz. For the ^{103}Rh spin pair system of **II**, the singlet–triplet mixing angle is given by $\theta_{\text{ST}} \approx 35^\circ$ in a field of 9.4 T.

The operator Q'_S is here called *quasi-singlet eigenorder* (QSEO), to emphasize its construction from the coherent Hamiltonian eigenstates and its close relationship with true singlet order Q_S . The operator Q'_S has also been called *singlet precursor order*,⁴⁰ since it is transformed adiabatically into singlet order by slow transport from high to low magnetic field.

The QSEO operator Q'_S is stable at high magnetic field (in the sense of not displaying coherent oscillations), only slowly decaying under dissipative processes. The decay of Q'_S may be described with a θ_{ST} -dependent time constant^{40,41} T'_S that is intermediate between the singlet time constant T_S and the magnetization relaxation time T_1 . In the current context, the QSEO Q'_S is prepared at high magnetic field and is converted adiabatically into singlet order Q_S at low magnetic field by sample transport. Conversely, singlet order Q_S in low magnetic field is transformed adiabatically into QSEO Q'_S when the sample is transported back into the high-field magnet.

There are many feasible methods for the preparation of QSEO.⁴⁰ In the current work, we prepare ^{103}Rh singlet order by DualPol and PulsePol sequences and then transform the singlet order into ^{103}Rh QSEO by the two-pulse sequence shown in Fig. 4. The transformation

$$Q_S \xrightarrow{S_2S'} Q'_S \quad (11)$$

is implemented by a sequence of two pulses and three free-evolution intervals, of the form

$$S_2S' = (\tau_1 - \pi_x - \tau_1 - \tau_2 - \pi_x - \tau_2). \quad (12)$$

The reverse transformation given by

$$Q'_S \xrightarrow{S'2S} Q_S \quad (13)$$

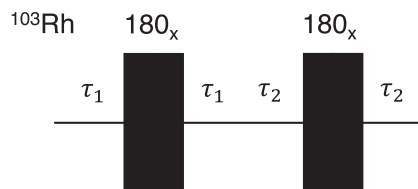


FIG. 4. S_2S' block for the transformation of ^{103}Rh singlet order into high-field ^{103}Rh quasi-singlet eigenorder [QSEO, see Eq. (8)], where $\tau_1 = 7.3 \text{ ms}$ and $\tau_2 = 27.6 \text{ ms}$. The black rectangles indicate BB1 composite π -pulses [Eq. (4)].

is implemented by the same sequence, but in reverse chronological order,

$$S'2S = (\tau_2 - \pi_x - \tau_2 - \tau_1 - \pi_x - \tau_1). \quad (14)$$

For the experiments described here, the intervals τ_1 and τ_2 take the values $\tau_1 = 7.3$ ms and $\tau_2 = 27.6$ ms, respectively. These values were obtained by numerical optimization for the spin system of isotopologue **II**, using the parameters given in Table I. Ignoring relaxation, numerical calculations predict 100% conversion of Q_S into Q'_S by the S2S' sequence, and the reverse for the S'S sequence.

III. RESULTS

A. NMR spectra

1. ^1H spectrum

The proton spectrum of the ^{18}O -labeled Rh formate solution is shown in Fig. 5. It features a single proton resonance split into a 1:2:1 triplet by J-couplings to the pair of ^{103}Rh nuclei (Fig. 5). The ^1H - ^{103}Rh J-coupling ($|^3J_{\text{HRh}}|$) is estimated to be 4.7 ± 0.1 Hz. There is no evidence of a $^2\Delta^1\text{H}(^{16}\text{O}, ^{18}\text{O})$ secondary isotope shift.

2. $^{13}\text{C}\{^1\text{H}, ^{103}\text{Rh}\}$ spectrum

The ^{13}C spectrum, acquired with both ^1H and ^{103}Rh decoupling, is shown in Fig. 6. It displays three peaks in an approximate 13:2:1 intensity ratio, corresponding to ^{13}C environments with different numbers of ^{18}O neighbors. The least shielded ("downfield") peak at 180.950 ppm is assigned to species ^{13}C sites, in which the ^{13}C atom is bound to two ^{16}O atoms. The central peak at 180.925 ppm corresponds to ^{13}C atoms bound to one ^{16}O atom and one ^{18}O atom. The most shielded ("upfield") peak at 180.900 ppm arises from ^{13}C atoms bound to two ^{18}O atoms.

The ^{13}C peak at ~ 180.950 ppm is more than 6 times as intense as the others. This is because it contains contributions from all four formate ligands of species **I** as well as from the three non-labeled formate ligands of species **II** and **III**. The peaks at ~ 180.925 and ~ 180.900 ppm, on the other hand, derive from just one formate ligand of species **II** and **III**, respectively.

The $^1\Delta^{13}\text{C}(^{16}\text{O}, ^{18}\text{O})$ secondary isotope shift is determined to be 3.8 ± 0.1 Hz or +25 ppb using the definition in Eq. (1).

This is of the same order as the $^1\Delta^{13}\text{C}(^{16}\text{O}, ^{18}\text{O})$ secondary isotope shifts found in many organic molecules.^{25–27}

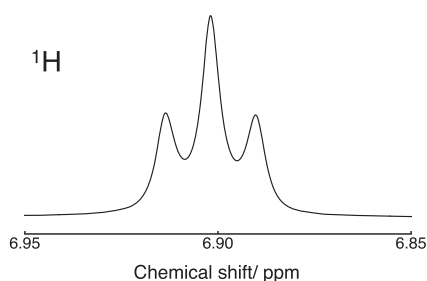


FIG. 5. ^1H NMR spectrum of a ~ 10 mM solution of ^{18}O -labeled rhodium formate in $\text{THF-}d_8$, acquired at 9.4 T and at 298 K. The spectrum is the result of one transient and was processed with 0.75 Hz Lorentzian line broadening.

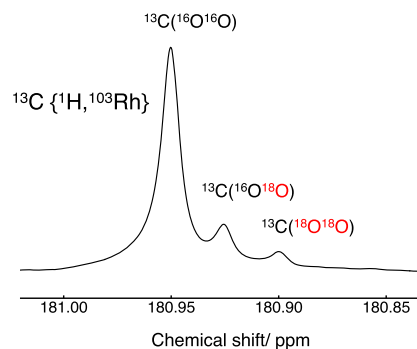


FIG. 6. Annotated $^{13}\text{C}\{^1\text{H}, ^{103}\text{Rh}\}$ NMR spectrum of a ~ 10 mM solution of ^{18}O labeled rhodium formate in $\text{THF-}d_8$, acquired at 14.1 T and at 298 K. The spectrum was acquired using 4096 transients and was processed using 1 Hz exponential line broadening. The acquisition time for this spectrum was ~ 22 h.

3. ^{103}Rh spectrum

The sequence shown in Fig. 7 was used for the acquisition of 2D ^1H - ^{103}Rh heteronuclear single-quantum (HSQC) spectra. After equilibration of the spin system in high magnetic field, DualPol is used to convert longitudinal ^1H polarization into longitudinal ^{103}Rh polarization (see Fig. 2 of Ref. 22). Next, ^{103}Rh transverse magnetization is generated by a ^{103}Rh 90° pulse. This transverse magnetization evolves during the incremented t_1 evolution interval. Transverse ^{103}Rh magnetization is returned to ^{103}Rh z-magnetization by another 90° pulse before being transferred to ^1H z-magnetization by a second DualPol block. A final 90° pulse on the ^1H channel generates transverse ^1H magnetization, which is detected in the subsequent t_2 interval, in the presence of ^{103}Rh decoupling. Double Fourier transformation of the $s(t_1, t_2)$ signal matrix leads to a two-dimensional spectrum with ^{103}Rh frequencies along the indirect frequency dimension and ^1H frequencies along the direct frequency dimension. An typical 2D spectrum is shown in Fig. 8. This shows a single narrow peak in the ^1H dimension and a six-peak structure in the ^{103}Rh dimension.

The ^{103}Rh spectrum is examined in more detail in Fig. 9. This may be interpreted as an AB quartet from the chemically inequivalent ^{103}Rh spin pair of isotopologue **II**, superposed on two singlet peaks from the magnetically equivalent ^{103}Rh spin pairs of isotopologues **I** and **III**.

Close examination of the bonding structures in Fig. 1 shows that the ^{103}Rh peak of isotopologue **III** is displaced from that

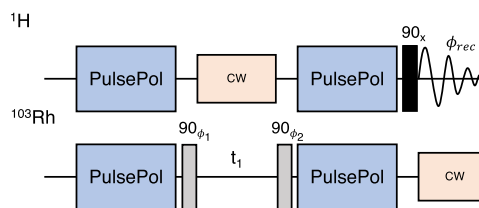


FIG. 7. Pulse sequence for the acquisition of 2D ^1H - ^{103}Rh spectra. Phase cycles are given by $\phi_1 = [x, x, -x, -x]$, $\phi_2 = [-x, x]$, and the receiver $\phi_{\text{rec}} = [x, -x, -x, x]$. The black rectangle indicates a BB1 composite $\pi/2$ pulse [Eq. (3)].

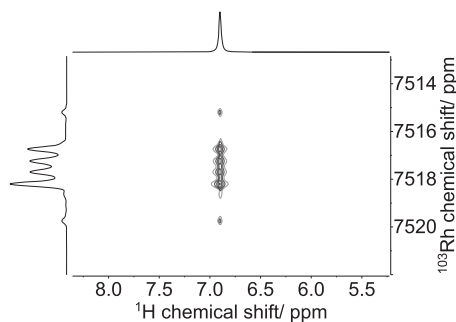


FIG. 8. Rhodium formate 2D HSQC spectrum of a ~ 10 mM solution of ^{18}O -labeled rhodium formate in $\text{THF-}d_8$ acquired at 9.4 T and at 298 K. The spectrum was processed with 2 Hz exponential line broadening in the directly detected F2 ^1H dimension and 0.75 Hz exponential line broadening in the F1 indirect ^{103}Rh dimension. The ^{103}Rh chemical shift is relative to the center of the ^{103}Rh peaks at 7517.5 ppm and the ^1H chemical shift is relative to the peak at 6.9 ppm. The acquisition time for this spectrum was ~ 11 h. The signs of the frequency axes take into account the positive magnetogyric ratio of ^1H , and the negative magnetogyric ratio of ^{103}Rh , according to Ref. 42.

of isotopologue **I** by the sum of the $^1\Delta^{103}\text{Rh}(^{16}\text{O}, ^{18}\text{O})$ and $^2\Delta^{103}\text{Rh}(^{16}\text{O}, ^{18}\text{O})$ secondary isotope shifts. Furthermore, the center frequency of the AB quartet from isotopologue **II** is at the exact midpoint of the **I** and **III** peaks. Hence, the one-bond and two-bond secondary isotope shifts may not be estimated independently from the spectrum in Fig. 9. Only the sum of the secondary isotope shifts is experimentally accessible and is estimated to be $^1\Delta^{103}\text{Rh}(^{16}\text{O}, ^{18}\text{O}) + ^2\Delta^{103}\text{Rh}(^{16}\text{O}, ^{18}\text{O}) = 1450 \pm 1$ ppb.

The ^{103}Rh - ^{103}Rh homonuclear J-coupling is taken directly from the outer splitting of the AB quartet of isotopologue **II** and is equal to $|^1J_{\text{RhRh}}| = 26.0 \pm 0.1$ Hz.

The $^{103}\text{Rh}\{^1\text{H}\}$ spectrum may be simulated assuming the following probabilities for the three isotopologues:

$$\begin{aligned} p(\text{I}) &= p(^{16}\text{O})^2, \\ p(\text{II}) &= 2p(^{16}\text{O})p(^{18}\text{O}), \\ p(\text{III}) &= p(^{18}\text{O})^2, \end{aligned} \quad (15)$$

where $p(^{16}\text{O}) + p(^{18}\text{O}) = 1$ and $p(^{18}\text{O})$ is the ^{18}O enrichment level of the single labeled formate ligand. Figure 9 (lower pane) shows a simulation with $p(^{18}\text{O}) = 0.45$. There is good agreement with the projection extracted from the experimental HSQC spectrum (top pane).

B. Singlet-filtered ^{103}Rh NMR

The ^{18}O -induced secondary isotope shifts break the magnetic equivalence of the ^{103}Rh spin pair in isotopologue **II**. This provides access to ^{103}Rh nuclear singlet order. We demonstrated this principle by converting ^1H -enhanced ^{103}Rh magnetization into singlet order, which was passed through a ^{103}Rh T_{00} filter, suppressing all other components of ^{103}Rh spin order, and regenerating the ^{103}Rh magnetization. The resulting $^{103}\text{Rh}\{^1\text{H}\}$ spectrum is shown in Fig. 10 and only displays signals from the AB quartet of isotopologue **II**. The ^{103}Rh NMR signals from isotopologues **I** and **III** are suppressed.

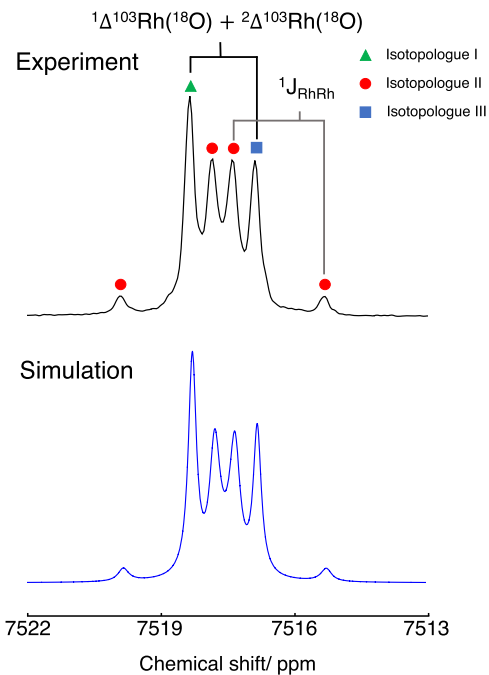


FIG. 9. Rhodium formate $^{103}\text{Rh}\{^1\text{H}\}$ experimental and simulated spectra. The experimental spectrum is a single slice of the indirect dimension of the 2D HSQC spectrum shown in Fig. 8 and was processed using 0.75 Hz line broadening. The simulated spectrum was produced assuming a previously reported ^{103}Rh T_2 for the rhodium formate complex of 181 ms,²² a ^{103}Rh spin pair chemical shift difference of 18.5 Hz, a $|^1J_{\text{RhRh}}|$ of 26.0 Hz, and an ^{18}O enrichment factor of 45%. The ^{103}Rh chemical shift is referenced to $(\Xi(^{103}\text{Rh})) = 3.16\%$. 1 Hz exponential line broadening was applied.

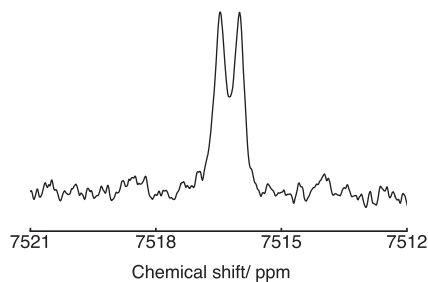


FIG. 10. Singlet-filtered $^{103}\text{Rh}\{^1\text{H}\}$ spectrum of a ~ 10 mM solution of ^{18}O -labeled rhodium formate in $\text{THF-}d_8$. The spectrum only displays peaks from isotopologue **II**. The data were acquired at 9.4 T using 2048 scans and at 298 K and processed with 1 Hz exponential line broadening. The ^{103}Rh chemical shift is referenced to $(\Xi(^{103}\text{Rh})) = 3.16\%$. The total acquisition time was ~ 24 h. The change in shift with respect to Fig. 9 is attributed to a ~ 0.7 K difference in sample temperature.

The experimental pulse sequence is shown in Fig. 11. Since this pulse sequence involves direct detection of the ^{103}Rh NMR signal, strong precautions were taken to suppress interference from acoustic ringing. The pulse sequence starts with a pair of 90° ^1H pulses. The indicated phase cycling of these pulses and the ^{103}Rh receiver selects for initial ^1H z-magnetization while suppressing acoustic ringing

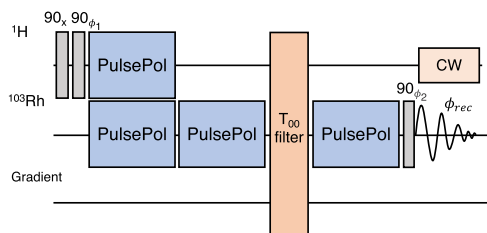


FIG. 11. Sequence used for the acquisition of ^{103}Rh singlet-filtered ^{103}Rh spectra. The initial pair of ^1H pulses, combined with the phase cycling, filters out acoustic ringing generated by the ^{103}Rh pulses. The phase cycles are given by $\phi_1 = [-x, x, -x, x]$, $\phi_2 = [x, x, x, x, y, y, y, y, -x, -x, -x, -x, -y, -y, -y, -y]$, and the receiver $\phi_{rec} = [x, -x, x, -x, y, -y, y, -y, -x, x, -x, x, -y, y, -y, y]$.

artifacts on the ^{103}Rh channel. A DualPol sequence of duration 100 ms converts ^1H z-magnetization into ^{103}Rh z-magnetization. A single-channel ^{103}Rh PulsePol sequence of duration 98 ms, as described in Sec. II D 2, converts the ^{103}Rh z-magnetization into ^{103}Rh singlet order. Signals not passing through ^{103}Rh singlet order are excluded by a dual-channel T_{00} filter sequence, as described in Sec. II D 3. This pulse sequence element further suppresses acoustic ringing interference on the ^{103}Rh channel. ^{103}Rh singlet order is returned back to ^{103}Rh z-magnetization by a second single-channel PulsePol block before being converted into ^{103}Rh transverse magnetization by a ^{103}Rh 90° pulse. The ^{103}Rh NMR signal is detected in the subsequent interval, in the presence of ^1H decoupling. Phase cycling suppresses signals from unwanted coherence transfer pathways and from acoustic ringing artifacts.

As expected, only the AB quartet belonging to isotopologue II is visible in the singlet-filtered ^{103}Rh spectrum shown in Fig. 10. The signals from isotopologues I and III are suppressed by the T_{00} filter, since singlet order cannot be generated in those magnetically equivalent systems. Since this spectrum was obtained by direct detection of the ^{103}Rh NMR signal, its signal-to-noise ratio is poor, as compared to the ^1H -detected ^{103}Rh spectrum shown in Fig. 9.

A shift difference of ~ 1 ppm is observed between the spectra in Figs. 9 and 10. This discrepancy is attributed to a small difference in sample temperature between the two experiments. From the known temperature dependence of the ^{103}Rh chemical shift,^{21,22} a temperature change of ~ 0.7 K is sufficient to explain the observed shift.

C. Relaxation of ^{103}Rh singlet order and quasi-singlet eigenorder

As described in Sec. II D 4, ^{103}Rh quasi-singlet eigenorder (QSEO), as described by the operator Q'_S [Eq. (8)], is expected to exhibit a non-oscillatory decay in high magnetic field. Furthermore, the QSEO may be transformed adiabatically into singlet order of the ^{103}Rh spin pair, described by the operator Q_S [Eq. (7)], by transport of the sample from high to low field.

1. Pulse sequence

The pulse sequence in Fig. 12 was used to study the relaxation of ^{103}Rh quasi-singlet eigenorder over a range of magnetic fields and the low-field relaxation of ^{103}Rh singlet order.

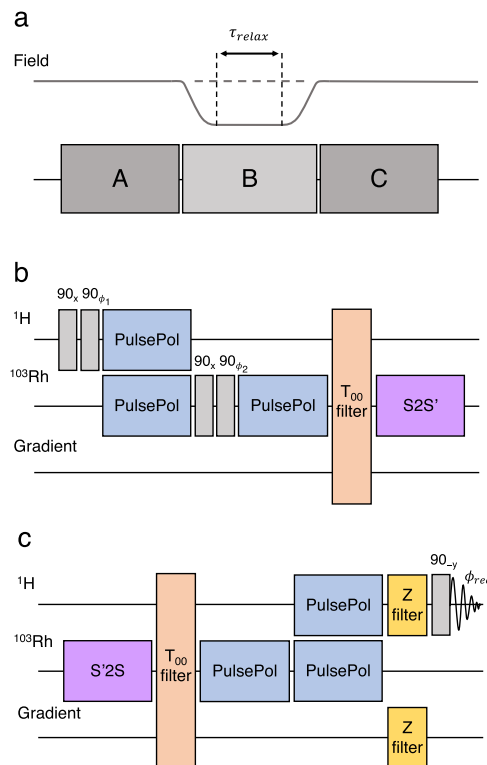


FIG. 12. Scheme used for studying the relaxation of ^{103}Rh quasi-singlet eigenorder, through detection of the ^1H signal. (a) The pulse sequence consists of blocks A, B, and C. Block A generates ^{103}Rh quasi-singlet eigenorder, starting from ^1H magnetization. Block B includes the optional transport of the sample to low magnetic field, a relaxation interval τ_{relax} , and transport of the sample back to high field. Block C converts the ^{103}Rh quasi-singlet eigenorder into observable ^1H magnetization. (b) The detailed structure of block A. (c) The detailed structure of block C. The phase cycles are given by $\phi_1 = [-x, x]$, $\phi_2 = [-x, -x, -x, -x, x, x, x, x]$, and the receiver $\phi_{rec} = [y, -y, y, -y, -y, y, -y, y]$.

The pulse sequence consists of three parts. The sequence in Part A [shown in Fig. 12(b)] generates the ^{103}Rh QSEO, starting from equilibrium ^1H magnetization. Part B consists of optional shuttling of the sample to low magnetic field, a relaxation interval τ_{relax} at the chosen field, and shuttling of the sample back into the high-field region of the magnet. The sequence in Part C [shown in Fig. 12(c)] converts the partially relaxed ^{103}Rh QSEO into an observable ^1H NMR signal.

Part A of the sequence [Fig. 12(b)] operates as follows: The initial pair of ^1H 90° pulses, combined with phase cycling, selects for longitudinal ^1H magnetization. A DualPol sequence of duration 100 ms converts ^1H z-magnetization into ^{103}Rh z-magnetization, which is selected for by a pair of ^{103}Rh 90° pulses, combined with phase cycling. These precautions ensure good suppression of final ^1H signals that do not pass through ^{103}Rh magnetization. A single-channel ^{103}Rh PulsePol sequence of duration 98 ms and symmetry $R4_1$, as described in Sec. II D 2, converts the ^{103}Rh z-magnetization into ^{103}Rh singlet order. Signals not passing through ^{103}Rh singlet order are excluded by a dual-channel T_{00} filter sequence, as

described in Sec. II D 3. Finally, the ^{103}Rh singlet order is converted into ^{103}Rh quasi-singlet eigenorder (QSEO) by a two-pulse $S2S'$ sequence, as described in Sec. II D 4.

Part B of the sequence consists of a variable relaxation interval τ_{relax} , optionally flanked by two transport intervals, during which the sample is transported to and from a region of low magnetic field. Although the QSEO operator Q'_S [Eq. (8)] is field-dependent, the relatively slow change in magnetic field induced by sample transport induces an adiabatic change in the Q'_S operator. Hence, it is possible to study the relaxation of Q'_S at any desired field by the procedure shown in part B of Fig. 12(a).

If the sample is transported into a sufficiently low magnetic field, the ^{18}O -induced chemical shift frequency difference between the ^{103}Rh nuclei becomes negligible, so that the ^{103}Rh spin pair becomes magnetically equivalent. Under these conditions, the QSEO operator Q'_S becomes identical to the singlet order operator Q_S [Eq. (7)]. Hence, the procedure in Fig. 12 allows study of the relaxation of ^{103}Rh singlet order, in low magnetic field.

Part C of the sequence [Fig. 12(c)] starts with a $S'S$ block (Sec. II D 4), which reconverts the ^{103}Rh QSEO into ^{103}Rh singlet order. This is selected for by another dual-channel T_{00} filter (Sec. II D 3). The dual T_{00} filter also destroys any residual proton magnetization generated during the waiting interval, thus suppressing unwanted ^1H background signals. ^{103}Rh singlet order is converted back into ^{103}Rh z-magnetization by a PulsePol block of symmetry $R4_1'$ (Sec. II D 2) before being converted into ^1H z-magnetization by a second DualPol block. Finally, the ^1H z-magnetization is selected for by a ^1H z-filter (Sec. II D 1) and converted into observable ^1H magnetization by a final 90° pulse.

2. Relaxation of ^{103}Rh QSEO in high field

The trajectory of indirectly detected ^{103}Rh QSEO in a field of 9.4 T is shown in Fig. 13(a). This was obtained by the pulse sequence in Fig. 12, but without the sample transport into low field. The trajectory fits well to a single-exponential decay with time constant $T'_S = 0.359 \pm 0.001$ s. This behavior confirms the preparation of the QSEO operator Q'_S by the pulse sequence and that the QSEO operator is an eigenoperator of the Liouvillian superoperator.

The time constant for QSEO decay T'_S may be compared with the time constant for the equilibration of longitudinal magnetization in the same field, $T_1 = 0.483 \pm 0.002$ s, as reported in Ref. 22. The relatively short value of T'_S may be attributed to the breaking of magnetic equivalence by the ^{18}O -induced isotope shifts in high magnetic field, lifting the protection of singlet order against many relaxation processes.

3. Relaxation of ^{103}Rh singlet order in low field

Transport of the sample into a sufficiently low magnetic field converts the high-field QSEO into low-field singlet order. Relaxation is allowed for an interval τ_{relax} , which is varied in a series of experiments. The remaining singlet order is determined by converting the singlet order back into QSEO adiabatic transport into high magnetic field, followed by conversion spin order into ^1H magnetization by the pulse sequence in Fig. 12(c).

At first sight, this experiment is unlikely to be feasible, since both transport intervals are ~ 1 s, i.e., much longer than the high-field relaxation time constant T'_S for QSEO, which is only ~ 0.36 s [see Fig. 13(a)]. However, as described in the supplementary

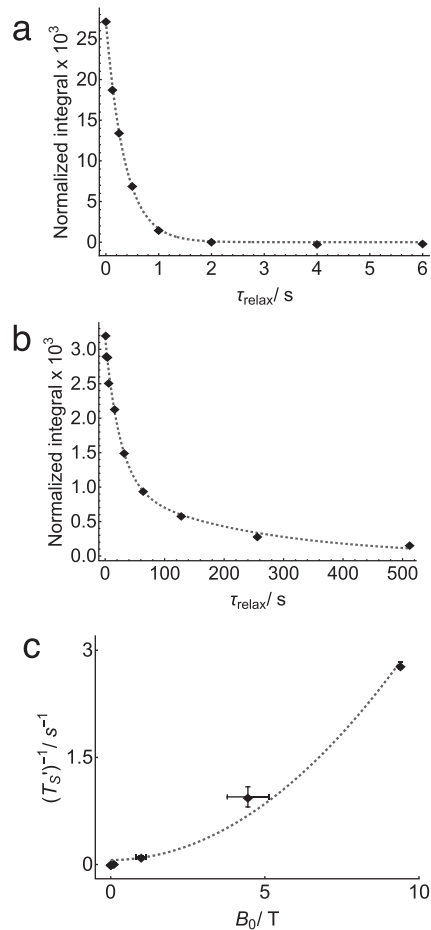


FIG. 13. (a) Decay curve for ^{103}Rh QSEO at a field of 9.4 T, obtained using the pulse sequence in Fig. 12, but without shuttling the sample to low field. The integrals are normalized against the ^1H spectrum obtained by a single ^1H 90° pulse applied to a system in thermal equilibrium at 9.4 T. The dashed line shows a monoexponential decay with time constant $T'_S = 0.359$ s. (b) Decay curve for ^{103}Rh QSEO at a field of 1 mT, obtained using the pulse sequence in Fig. 12, including the shuttling of the sample to low field. The dashed line shows a bi-exponential decay of the form $A \exp\{-t/T_a\} + B \exp\{-t/T_b\}$, where $A = 2.6 \times 10^{-3}$, $B = 5.5 \times 10^{-3}$, $T_a = 229$ s, and $T_b = 25.2$ s. (c) ^{103}Rh QSEO relaxation rate constant $(T'_S)^{-1}$ as a function of magnetic field strength B . The dashed line shows the quadratic function $(T'_S)^{-1}(B) = (T'_S)^{-1}(0) + aB^2$, where $(T'_S)^{-1}(0) = 0.063$ s $^{-1}$ and $a = 0.031$ s $^{-1}$ T $^{-2}$.

material, the transport trajectory for the sample from high to low field leads to a magnetic field that is almost constant for the first ~ 0.35 s, followed by a very rapid decrease in magnetic field to ~ 1 mT, where it remains for the rest of the transport interval. Since the rate constant $(T'_S)^{-1}$ has an approximately quadratic dependence on magnetic field, the rapid decrease in magnetic field after the first ~ 0.36 s of the transport trajectory leads to a near-suspension of QSEO relaxation after this point. The reverse occurs when the sample is transported back into high field. Hence, the two transport intervals of ~ 1 s only lead to effectively ~ 0.7 s of spin order decay.

This does lead to a significant loss of signal but not so large as to make the experiment unfeasible.

The experimental relaxation trajectory for ^{103}Rh singlet order in the low magnetic field of 1 mT is shown in Fig. 13(b). Surprisingly, the low-field ^{103}Rh singlet order decay is distinctly non-exponential. The trajectory fits well to a bi-exponential decay function of the form $A \exp\{-t/T_a\} + B \exp\{-t/T_b\}$, where $A = (2.6 \pm 0.8) \times 10^{-3}$, $B = (5.5 \pm 0.8) \times 10^{-3}$, $T_a = 229 \pm 94$ s, and $T_b = 25.2 \pm 5.8$ s. The A and B coefficients are very small, since the amplitudes are normalized against thermal ^1H magnetization.

We attribute the longer decay constant T_a to the decay of rhodium singlet order ($T_a = T_S$). This may be compared with the time constant for the equilibration of longitudinal magnetization in the same field, $T_1 = 28.2 \pm 1.2$ s, as reported in Ref. 22. The low-field rhodium singlet lifetime is ~ 8 times longer than the corresponding rhodium T_1 and thus constitutes a long-lived state in the low field.

The reduced signal amplitude for the low-field measurement of ^{103}Rh T_S , relative to the high-field measurement of T'_S , is well accounted for by relaxation losses during shuttling, as shown in the supplementary material.

4. Field-dependence of ^{103}Rh QSEO relaxation

Repetition of the sequence in Fig. 12, while varying the end position of the sample shuttle, allows the determination of the QSEO decay time constant T'_S as a function of magnetic field.

The experimentally determined field-dependence of the rate constant $(T'_S)^{-1}$ is shown in Fig. 13(c). The large horizontal error bars on the magnetic field at the $B \sim 5$ T point are due to the large gradient of the magnet stray field over the sample dimensions at this location. The ^{103}Rh QSEO decay rate constant $(T'_S)^{-1}$ increases approximately quadratically with the magnetic field B . The field-dependent relaxation rate constant is a reasonable fit to the quadratic function $(T'_S)^{-1}(B) = (T'_S)^{-1}(0) + aB^2$, where $(T'_S)^{-1}(0) = 0.063 \pm 0.055 \text{ s}^{-1}$ and $a = 0.031 \pm 0.002 \text{ s}^{-1} \text{ T}^{-2}$.

IV. DISCUSSION

Selective ^{18}O labeling of the dirhodium formate paddlewheel complex successfully breaks the magnetic equivalence of the ^{103}Rh sites, enables the estimation of the one-bond ^{103}Rh – ^{103}Rh J-coupling, and provides access to long-lived ^{103}Rh singlet order. We find that the sum of one- and two-bond ^{103}Rh (^{16}O , ^{18}O) secondary isotope shifts is equal to 1450 ± 1 ppb in the rhodium formate paddlewheel complex. The one-bond ^{18}O -induced ^{103}Rh secondary isotope shift is ~ 50 times larger than the corresponding ^{18}O -induced secondary isotope shift of ^{13}C . This reflects the high sensitivity of the ^{103}Rh chemical shift to the local chemical environment. To our knowledge, this is the first measurement of ^{103}Rh (^{16}O , ^{18}O) isotope shifts. This particular type of shift has received recent interest,^{43–45} although ^{103}Rh secondary isotope shifts induced by other isotopic substitutions have been reported before.^{13,43,46–50}

Reports of ^{103}Rh – ^{103}Rh J-couplings are rare. The only previous reports have been in highly asymmetric complexes.^{15,16,24,51,52} The selective ^{18}O labeling unveils the otherwise inaccessible one-bond ^{103}Rh – ^{103}Rh J-coupling in the *symmetric* rhodium formate paddlewheel complex. The one-bond J -coupling can be used to characterize the strength and nature of the chemical bond between coupled

nuclei.^{53,54} Solvents act as axial ligands for rhodium paddlewheel complexes,²¹ which profoundly affects the character of the Rh–Rh bond² and, by extension, catalytic performance.¹⁹ Investigations of solvent effects on the ^{103}Rh – ^{103}Rh J-coupling are now under way.

The singlet-filtered ^{103}Rh spectrum shown in Fig. 10 demonstrates the successful generation of ^{103}Rh – ^{103}Rh singlet order in the ^{18}O -labeled rhodium formate paddlewheel complex. As far as we know, this is the first time a nuclear singlet state has been accessed for elements beyond the third row of the periodic table.

^{103}Rh singlet order was successfully converted into ^{103}Rh quasi-singlet eigenorder, which decays exponentially in high magnetic field. The ^{103}Rh relaxation rate constant T'_S has a quadratic dependence on the magnetic field B_0 , with an additional zero-field contribution of $T'_S(0) = 0.063 \pm 0.055 \text{ s}^{-1}$. The quadratic field-dependence is consistent with a dominant chemical shift anisotropy (CSA) relaxation mechanism. Indeed, the ^{103}Rh chemical shift anisotropy has been estimated to be ~ 9900 ppm in this compound.²² The molecular symmetry constrains the two ^{103}Rh CSA tensors to be identical in both magnitude and orientation for the case of a symmetrical molecular geometry respecting inversion symmetry. In this case, the CSA mechanism should be ineffective for singlet relaxation, which is sensitive to the difference between the CSA tensors. Nevertheless, thermal fluctuations of the geometry, or ligand exchange at the axial sites, may cause breakdown of this cancellation mechanism.

The high-field ^{103}Rh quasi-singlet eigenorder relaxation time constant T'_S of 0.359 ± 0.01 s is shorter than the corresponding high-field ^{103}Rh T_1 relaxation time constant of 0.482 ± 0.002 s. This suggests that modulation of the ^{103}Rh isotropic chemical shifts by chemical exchange at the axial sites also contributes to the singlet relaxation. It has been shown that chemical exchange can be a potent singlet relaxation mechanism even when the exchange kinetics are slow.²⁶

The very low γ of ^{103}Rh , combined with the high formal symmetry of the rhodium formate paddlewheel complex, endowed with a local inversion center at the center of the Rh–Rh bond, suggests the possibility of ^{103}Rh – ^{103}Rh singlet order with an extremely long lifetime, perhaps exceeding the observed ~ 1 h lifetime for $^{13}\text{C}_2$ singlet order in a suitable molecular vehicle.⁵⁵ However, these expectations were not borne out in practice. Although the low-field ^{103}Rh T_S is ~ 8 times longer than the corresponding low-field ^{103}Rh T_1 , the ^{103}Rh singlet lifetime for the rhodium formate paddlewheel complex of $T_S \sim 230$ s is not exceptional.

At the time of writing, the mechanism for ^{103}Rh singlet relaxation in low magnetic field is not well understood. Well-known mechanisms, such as the modulation of ^1H – ^{103}Rh or ^{103}Rh – ^{103}Rh dipole–dipole couplings by molecular tumbling are far too weak. One candidate is spin-rotation, which is field-independent, and which has been proposed before as a mechanism for low-field ^{103}Rh T_1 relaxation.^{22,56} However, the high degree of molecular symmetry for Rh formate should cause this mechanism to cancel out substantially for the relaxation of ^{103}Rh singlet order. The inversion symmetry about the center of the Rh–Rh bond constrains the spin-rotation tensors for the two ^{103}Rh sites to be identical in the equilibrium molecular structure, in a fashion similar to that of the CSA tensors. Hence, the spin-rotation mechanism should cancel for tumbling molecules that retain a perfectly symmetrical geometry. Nevertheless, fluctuations in the local molecular geometry, through

thermal geometry distortions, or ligand exchange, could permit a significant spin-rotation contribution to the singlet relaxation rate constant T_S^{-1} .

The bi-exponential decay of ^{103}Rh singlet order in low magnetic field is also currently unexplained; however, bi-exponential low-field decay of long-lived spin order is not uncommon and has been reported before for ^1H and ^{13}C spin pairs.^{40,41} There is also a possibility that slow axial ligand exchange could contribute to low-field ^{103}Rh singlet relaxation. Chemical exchange could also induce fluctuations of the ^{103}Rh – ^{103}Rh J-coupling, which might also induce singlet–triplet transitions and hence the relaxation of ^{103}Rh singlet order. There is also the possibility that nonadiabatic spin transitions during the sample transport could contribute to the observed bi-exponentiality. However, as shown in the supplementary material, the adiabaticity criterion appears to be well satisfied in the current case.

SUPPLEMENTARY MATERIAL

The supplementary material contains details on (i) the chemical synthesis; (ii) the shuttling trajectory; (iii) an analysis of spin order loss during shuttling; and (iv) an examination of the adiabaticity of the field-cycling.

ACKNOWLEDGMENTS

We acknowledge funding from the European Research Council (Grant No. 786707-FunMagResBeacons), and EPSRC-UK (Grant Nos. EP/P009980/1, EP/P030491/1, and EP/V055593/1). M.L. acknowledges financial support by the Max-Planck-Gesellschaft and the Max-Planck-Institut für Kohlenforschung.

We thank Alexander A. Auer and Kostya Ivanov for insightful discussions and Alexey Kiryutin for sharing his designs for the sample shuttle. We thank Fabio P. Caló for important input on the synthesis of the complexes.

AUTHOR DECLARATIONS

Conflict of Interest

The authors have no conflicts to disclose.

Author Contributions

Harry Harbor-Collins: Conceptualization (equal); Data curation (equal); Formal analysis (equal); Investigation (equal); Methodology (equal); Software (equal); Validation (equal); Visualization (equal); Writing – original draft (equal); Writing – review & editing (equal).

Mohamed Sabba: Conceptualization (supporting); Data curation (equal); Formal analysis (equal); Investigation (equal); Methodology (equal); Resources (equal); Software (equal); Validation (equal); Visualization (equal); Writing – original draft (equal); Writing – review & editing (equal). **Christian Bengs:** Formal analysis (lead); Methodology (equal); Software (lead); Writing – review & editing (equal). **Gamal Moustafa:** Conceptualization (equal); Investigation (equal); Resources (lead); Validation (equal); Visualization (equal). **Markus Leutzsch:** Conceptualization (lead); Supervision (equal); Visualization (equal); Writing – review & editing (equal). **Malcolm H. Levitt:** Conceptualization (equal); Formal analysis

(equal); Funding acquisition (equal); Project administration (equal); Resources (equal); Supervision (equal); Writing – original draft (equal); Writing – review & editing (equal).

DATA AVAILABILITY

The data that support the findings of this study are available from the corresponding author upon reasonable request.

APPENDIX: SINGLET ORDER GENERATION

As discussed previously,³⁵ the first-order average Hamiltonian $\bar{H}_\Delta^{(1)}$, of a symmetry-based sequence engineered for selective excitation of singlet order from longitudinal magnetization has the general form

$$\begin{aligned} \bar{H}_\Delta^{(1)} = \omega_{\text{nut}}^{ST} \frac{1}{2} \{ & |S_0\rangle\langle T_{\pm 1}| \exp(-i\phi_{ST}) \\ & + |T_{\pm 1}\rangle\langle S_0| \exp(+i\phi_{ST}) \}. \end{aligned} \quad (\text{A1})$$

The singlet and triplet states are defined in Eq. (6). The choice of \pm sign depends upon the symmetry numbers of the pulse sequence, as described in Ref. 35. The phase factor ϕ_{ST} and singlet–triplet nutation frequency ω_{nut}^{ST} depend on the R-element of the symmetry-based pulse sequence.

The phase ϕ_{ST} is not relevant in the current context. The Rabi frequency of population transfer from either of the $|T_{\pm 1}\rangle$ states to $|S_0\rangle$ is proportional to the chemical shift difference $\omega_\Delta = 2\pi\Delta$ and the magnitude of the scaling factor κ as follows:

$$\omega_{\text{nut}}^{ST} = \omega_\Delta |\kappa|. \quad (\text{A2})$$

Maximal generation of singlet order is achieved when the total excitation time τ_{opt} is

$$\tau_{\text{opt}} = \frac{\pi}{\omega_{\text{nut}}^{ST}} = \frac{\pi}{\omega_\Delta |\kappa|}. \quad (\text{A3})$$

In the context of singlet–triplet conversion, a RN_n^v sequence is realized as a series of discrete R-elements, each of duration $\tau_R = n/(NJ)$, such that the optimal number of R-elements for singlet excitation, n_{opt} , is

$$n_{\text{opt}} \approx \frac{\pi}{\omega_\Delta \tau_R |\kappa|} = \cot(\theta_{ST}) \frac{N}{2n|\kappa|}, \quad (\text{A4})$$

where we have used the relation $\cot(\theta_{ST}) = J/\Delta$, from Eq. (10).

In general, the scaling factor κ depends on the choice of R-element. For an RN_n^v sequence constructed from the PulsePol R-element,³⁵ such as that used in this paper, we have

$$|\kappa| = \sqrt{2} \frac{N}{n\pi} \sin^2\left(\frac{\pi n}{2N}\right). \quad (\text{A5})$$

The previous two equations may be combined to obtain

$$n_{\text{opt}}^{\text{PulsePol}} \approx \frac{\pi}{2\sqrt{2}} \cot(\theta_{ST}) \csc^2\left(\frac{\pi n}{2N}\right). \quad (\text{A6})$$

In practice, the sequence is implemented as L repetitions of R-element pairs (see Fig. 2), such that the optimal number of repetitions is given by

$$L_{\text{opt}} = \text{round}\left(\frac{\pi}{4\sqrt{2}} \cot(\theta_{\text{ST}}) \csc^2\left(\frac{\pi n}{2N}\right)\right). \quad (\text{A7})$$

This is the equation that appears in the paper.

This expression only depends on the singlet–triplet mixing angle θ_{ST} and the ratio of symmetry numbers n/N . Beyond near-equivalence, as θ_{ST} grows larger, maximal singlet excitation is only possible with a compensatory decrease in n/N . This may be readily accomplished by using sequences in the family $RN_1^{(N/2)-1}$, the simplest member of which is $R4_1^1$.

REFERENCES

- S. Lin and C. Turro, *Chem. - Eur. J.* **27**, 5379 (2021).
- R. Hrdina, *Eur. J. Inorg. Chem.* **2021**, 501.
- J. Hansen and H. M. L. Davies, *Coord. Chem. Rev.* **252**, 545 (2008).
- A. Abshire, D. Moore, J. Courtney, and A. Darko, *Org. Biomol. Chem.* **19**, 8886 (2021).
- B. G. Anderson, D. Cressy, J. J. Patel, C. F. Harris, G. P. A. Yap, J. F. Berry, and A. Darko, *Inorg. Chem.* **58**, 1728 (2019).
- Z. Li, H. Jiang, J. Liu, T. Ning, N. T. S. Phan, and F. Zhang, *ACS Appl. Mater. Interfaces* **14**, 30714 (2022).
- A. F. Trindade, J. A. S. Coelho, C. A. M. Afonso, L. F. Veiros, and P. M. P. Gois, *ACS Catal.* **2**, 370 (2012).
- B. Zhu, G. Liu, L. Chen, L. Qiu, L. Chen, J. Zhang, L. Zhang, M. Barboiu, R. Si, and C.-Y. Su, *Inorg. Chem. Front.* **3**, 702 (2016).
- E. B. Boyar and S. D. Robinson, *Coord. Chem. Rev.* **50**, 109 (1983).
- A. Erck, L. Rainen, J. Whitleyman, I.-M. Chang, A. P. Kimball, and J. Bear, *Exp. Biol. Med.* **145**, 1278 (1974).
- M. Fandzloch, A. W. Augustyniak, L. Dobrzańska, T. Jędrzejewski, J. Sitkowski, M. Wypij, and P. Golińska, *J. Inorg. Biochem.* **210**, 111072 (2020).
- J. Ohata and Z. T. Ball, *Dalton Trans.* **47**, 14855 (2018).
- L. Carlton, in *Annual Reports on NMR Spectroscopy*, edited by G. A. Webb (Academic Press, 2008), Vol. 63, pp. 49–178.
- F. A. Cotton, E. A. Hillard, and C. A. Murillo, *J. Am. Chem. Soc.* **124**, 5658 (2002).
- P. Caddy, M. Green, L. E. Smart, and N. White, *J. Chem. Soc., Chem. Commun.* **1978**(19), 839.
- J. L. Cunningham and S. B. Duckett, *Dalton Trans.* **2005**(4), 744.
- M. Szabó, M. Kleineisel, K. Németh, A. Domján, E. Vass, and G. Szilvgyi, *Chirality* **32**, 446 (2020).
- M. C. Pirrung, H. Liu, and A. T. Morehead, *J. Am. Chem. Soc.* **124**, 1014 (2002).
- C. J. Laconsay, A. Pla-Quintana, and D. J. Tantillo, *Organometallics* **40**, 4120 (2021).
- X. Tang, H. Noda, and M. Shibasaki, *Angew. Chem.* **135**, e202311027 (2023).
- F. P. Caló, G. Bistoni, A. A. Auer, M. Leutzsch, and A. Fürstner, *J. Am. Chem. Soc.* **143**, 12473 (2021).
- H. Harbor-Collins, M. Sabba, G. Moustafa, B. Legrady, M. Soundararajan, M. Leutzsch, and M. H. Levitt, *J. Chem. Phys.* **159**, 104307 (2023).
- J. G. J. Norman and H. J. Kolari, *J. Am. Chem. Soc.* **100**, 791 (1978).
- C. D. Garner, M. Berry, and B. E. Mann, *Inorg. Chem.* **23**, 1500 (1984).
- M. C. D. Tayler and M. H. Levitt, *J. Am. Chem. Soc.* **135**, 2120 (2013).
- C. Bengs, L. Dagys, G. A. I. Moustafa, J. W. Whipham, M. Sabba, A. S. Kiryutin, K. L. Ivanov, and M. H. Levitt, *J. Chem. Phys.* **155**, 124311 (2021).
- P. E. Hansen, *Prog. Nucl. Magn. Reson. Spectrosc.* **20**, 207 (1988).
- I. V. Zhukov, A. S. Kiryutin, A. V. Yurkovskaya, Y. A. Grishin, H.-M. Vieth, and K. L. Ivanov, *Phys. Chem. Chem. Phys.* **20**, 12396 (2018).
- S. Wimperis, *J. Magn. Reson., Ser. A* **109**, 221 (1994).
- H. K. Cummins, G. Llewellyn, and J. A. Jones, *Phys. Rev. A* **67**, 042308 (2003).
- I. Schwartz, J. Scheuer, B. Tratzmiller, S. Müller, Q. Chen, I. Dhand, Z.-Y. Wang, C. Müller, B. Naydenov, F. Jezek, and M. B. Plenio, *Sci. Adv.* **4**, eaat8978 (2018).
- B. Tratzmiller, “Pulsed control methods with applications to nuclear hyperpolarization and nanoscale NMR,” Ph.D. thesis, Universität Ulm, 2021.
- G. A. Morris and R. Freeman, *J. Am. Chem. Soc.* **101**, 760 (1979).
- D. P. Burum and R. R. Ernst, *J. Magn. Reson.* **39**, 163 (1980).
- M. Sabba, N. Wili, C. Bengs, J. W. Whipham, L. J. Brown, and M. H. Levitt, *J. Chem. Phys.* **157**, 134302 (2022).
- M. Carravetta, M. Edén, X. Zhao, A. Brinkmann, and M. H. Levitt, *Chem. Phys. Lett.* **321**, 205 (2000).
- M. C. D. Tayler, (2020).
- G. Pileio, *Prog. Nucl. Magn. Reson. Spectrosc.* **98–99**, 1 (2017).
- G. Pileio and M. H. Levitt, *J. Chem. Phys.* **130**, 214501 (2009).
- M. Sabba, “Generalized methodology for control of long-lived nuclear spin order in magnetic resonance,” Ph.D. thesis, University of Southampton, 2023.
- A. S. Kiryutin, M. S. Panov, A. V. Yurkovskaya, K. L. Ivanov, and G. Bodenhausen, *ChemPhysChem* **20**, 766 (2019).
- M. H. Levitt, *J. Magn. Reson.* **126**, 164 (1997).
- K. R. Koch and L. Engelbrecht, *Dalton Trans.* **46**, 9303 (2017).
- J. C. Davis, M. Bühl, and K. R. Koch, *J. Phys. Chem. A* **117**, 8054 (2013).
- J. C. Davis, “Understanding the origin of $^{35/37}\text{Cl}$ and $^{16/18}\text{O}$ isotope effects on ^{195}Pt and ^{103}Rh NMR nuclear shielding in selected Pt(IV) and Rh(III) complexes: A DFT study,” Ph.D. thesis, Stellenbosch University, Stellenbosch, 2013.
- A. Salzer, T. Eglolf, and W. Von Philipsborn, *Helv. Chim. Acta* **65**, 1145 (1982).
- B. E. Mann, N. J. Meanwell, C. M. Spencer, B. F. Taylor, and P. M. Maitlis, *J. Chem. Soc., Dalton Trans.* **1985**(8), 1555.
- T. E. Geswindt, W. J. Gerber, D. J. Brand, and K. R. Koch, *Anal. Chim. Acta* **730**, 93 (2012).
- J. Ruiz, B. E. Mann, C. M. Spencer, B. F. Taylor, and P. M. Maitlis, *J. Chem. Soc., Dalton Trans.* **1987**(8), 1963.
- D. Nanz, W. V. Philipsborn, U. E. Bucher, and L. M. Venanzi, *Magn. Reson. Chem.* **29**, S38 (1991).
- A. L. Davis and R. J. Goodfellow, *J. Chem. Soc., Dalton Trans.* **1993**(15), 2273.
- E. Maurer, S. Rieker, M. Schollbach, A. Schwenk, T. Eglolf, and W. von Philipsborn, *Helv. Chim. Acta* **65**, 26 (1982).
- M. Dračinský, in *Annual Reports on NMR Spectroscopy*, edited by G. A. Webb (Academic Press, 2017), Vol. 90, pp. 1–40.
- T. Bräuniger, S. Ghedia, and M. Jansen, *Z. Anorg. Allg. Chem.* **636**, 2399 (2010).
- G. Stevanato, J. T. Hill-Cousins, P. Håkansson, S. S. Roy, L. J. Brown, R. C. D. Brown, G. Pileio, and M. H. Levitt, *Angew. Chem.* **127**, 3811 (2015).
- A. J. Vega, P. A. Beckmann, S. Bai, and C. Dybowski, *Phys. Rev. B* **74**, 214420 (2006).